JMEPEG (1993) 2:819-838

A Numerical Model for Deep Penetration Welding Processes

S.G. Lambrakos, E.A. Metzbower, P.G. Moore, J.H. Dunn, and A. Monis

The general features of a numerical model, and of its extensions, for calculating the temperature and fluid velocity field in a three-dimensional workpiece undergoing deep penetration laser beam welding are described. In the current model, the deposition of power from the beam is represented by time-dependent boundary conditions on the equations of energy and momentum transfer. These boundary conditions are specified at each timestep on a surface whose configuration can change with time and upon which energy is deposited according to a specified power distribution. This model also includes the effects of the buoyancy force on the melt pool and of the surface tension gradient on the surface of the fluid. The coupled equations of energy, momentum transfer, and continuity combined with the time-dependent boundary conditions representing the keyhole and the moving boundaries of the workpiece are solved by using a specific implementation of the SIMPLE algorithm. The important features of the numerical methods used in the model are discussed. Isotherms and convection patterns calculated using the current model are presented, and their significance for predicting weldment properties is discussed. A significant result of the simulations is that they demonstrate the overwhelming influence of the keyhole vapor/liquid interface on fluid convection and conduction in deep penetration welding.

Keywords
numerical modeling, keyhole stirring, deep penetration, partioning

1. Introduction

THE nature of fluid convection in a weld pool can have a significant effect on the properties of the associated weld. It is the combined influence of fluid convection and heat transfer for a given welding process that determines the temperature history of the workpiece and thus the microstructure of its various segments. In the case of arc welding processes, there have been significant contributions to the modeling of fluid convection and heat transfer in the workpiece.[1-3] Calculations using these models have contributed to a quantitative understanding of the relative influences of the electromagnetic force, surface tension, and buoyancy force on fluid convection in the weld pool.

Deep penetration laser welding differs from other conventional welding processes in that energy deposition does not occur on the surface of the workpiece or over some contiguous spatial distribution within the workpiece. Instead, for deep penetration welding, energy deposition occurs on the surface boundary of a keyhole that moves, on average, through the workpiece at a constant speed, i.e., the welding speed. In general, the region inside the keyhole is made of turbulent and oscillatory fluid structures that exist in a gas phase. Although the boundary of the keyhole fluctuates in time, and may periodically collapse,[4] for a given beam intensity and speed, it can be characterized on average by a fixed surface configuration extending into the melt pool. Because the three-dimensional distribution of temperature in the neighborhood of the keyhole is correlated with the time-averaged steady-state shape of the liquid/vapor interface defining the keyhole, an approximate representation of the keyhole is obtained using a distributed heat source extending into the workpiece. Notable among distributions used for representing the distribution of heat in the workpiece is the modified Beer-Lambert's law.[5-7] The function representing the distribution of heat in the workpiece can be adopted as the source term in the heat conduction equation. This approach has been used effectively for modeling heat conduction in the workpiece for steady-state conditions.[5-8]

It is observed experimentally that the presence of a moving keyhole has a major influence on the fluid flow in the weld pool in the neighborhood of the keyhole boundary. It is conjectured that this influence is due to the mechanical action of the vapor/liquid interface moving through the molten pool. The spatial distribution of energy deposited on the surface of the keyhole (i.e., the vapor/liquid interface defining the keyhole boundary) is a complicated function of time, the instantaneous configuration of the keyhole, the gas phase processes occurring inside the keyhole, and the spatial and temporal characteristics of the laser beam. On average with respect to time, however, a Gaussian power distribution should be a reasonable approximation of the energy deposition on the surface of the keyhole relative to the center of the beam.

A numerical model is described for deep penetration laser welding that explicitly considers the influence of the keyhole liquid/vapor interface on convection. The influence of the keyhole is represented in the model by time-dependent boundary conditions on the equations of energy and momentum transfer. These boundary conditions are specified at each timestep on a dynamically evolving liquid/vapor interface whose configuration is a function of the energy deposited on it and the material properties of the workpiece. In the model, the rate and spatial distribution of energy deposition on the surface of the keyhole boundary is specified according to a Gaussian power law distribution. The motion of the workpiece with respect to the beam is

S.G. Lambrakos, E.A. Metzbower, P.G. Moore, and **J.H. Dunn,** Code 6324, Naval Research Laboratory, Washington, DC 20375-5000.
A. Monis, University of Maryland, College Park, MD.

represented by time-dependent boundary conditions on the energy transport equations. As the workpiece moves past the beam, the forward face is always at the ambient temperature, T_A. Thus, a thermal cycle can be calculated for any point (x, y, and z) in the workpiece, i.e., $T(x, y, z, t)$, where $t_L < t < t_U$, and t_L and t_U define the beginning and end of the cycle. Discretization of the equations defining this model system is via a specific implementation of the SIMPLE (semi-implicit method for pressure-linked equations) algorithm.[9] The SIMPLE algorithm for the numerical solution of the coupled transport equations has been used successfully for modeling energy transfer and fluid flow in welding processes. This method was chosen because its formalism provides flexibility for introducing extensions consistent with a specific process to be simulated. The general formalism of the SIMPLE algorithm is in terms of physical quantities that are defined with respect to cubical volume elements. Because this mathematical framework is not *a priori* structured for use with any particular method of solving the discretization equations, one may use methods based on the physical aspects of the problem to optimize the algorithm for a specific computer architecture. This formulation has significance in terms of convenience and flexibility for extending this model for the calculation of welding structures associated with inclusions or asymmetric unsteady structures. In the model, a formulation of the SIMPLE algorithm was constructed according to the specific aspects of simulating deep penetration welding processes. The formulation of the SIMPLE algorithm does not give explicit consideration to any particular numerical procedure for calculating derivatives. This formulation is motivated by the increased availability of computer memory, which permits the use of more convenient forms of discretization equations, i.e., forms that previously may have been considered inefficient.

Included in this article is a discussion of the significance of the influence of the keyhole on thermal cycles associated with deep penetration welding processes and of potential extensions of the model for the analysis of different types of welding structures. A significant result of the simulations is that they demonstrate the overwhelming influence of the stirring action due to the keyhole vapor/liquid interface on fluid convection in the weld pool. The nature of this influence is discussed relative to other driving forces of convection in the weld pool. Also included in this article is a case study for predicting an estimate of thermal cycles for positions within a workpiece for welding of iron or low-carbon steels.

2. Physical Model of Deep Penetration Laser Welding Process

2.1 *Coupled Transport Equations and Forcing Terms*

The model system to be specified is that of unsteady energy and momentum transport in a coordinate system that is fixed in the reference frame of a moving laser beam energy source. A schematic of the model system is shown in Fig. 1. The boundaries of the model system are defined, at each timestep, by the sides of a finite-sized rectangular workpiece and by the temperature of vaporization isotherm, which defines the boundary of the keyhole.

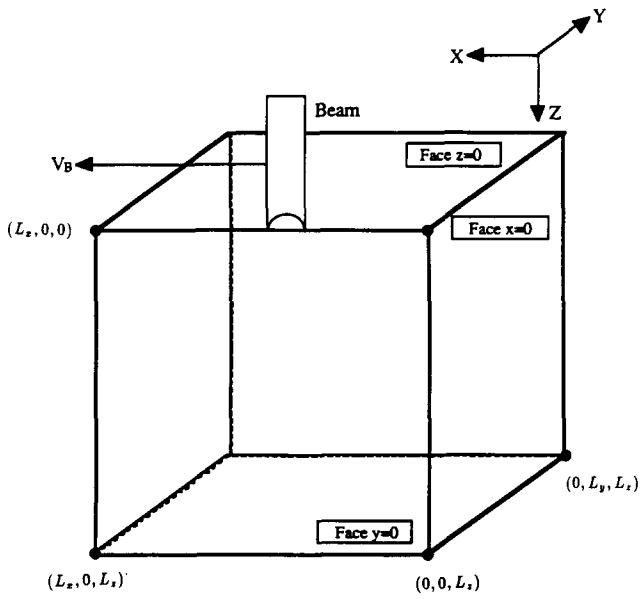

Fig. 1 Schematic of model system showing relative coordinates of system boundaries.

The system is assumed to be symmetric about the xz face at $y = 0$ (see Fig. 1); thus, only one half of the system is modeled. The equations governing the model system are

$$\rho C_p(T)\frac{\partial T}{\partial t} + \nabla \cdot [\rho C_p(T)\mathbf{U}T] + \rho\delta_{1j}V_B\frac{\partial (C_p(T)T)}{\partial x_j} = \nabla \cdot [k(T)\nabla\, T(x,t)] \quad [1]$$

$$\rho\frac{\partial U_j}{\partial t} + \nabla \cdot (\rho\mathbf{U}U_j) + \rho\delta_{1j}V_B\frac{\partial U_j}{\partial x_j} = \nabla \cdot [\mu(T)\nabla U_j] - \frac{\partial P}{\partial x_j} + B_j \quad [2]$$

and

$$\nabla \cdot \mathbf{U} = 0 \quad [3]$$

where $j = 1, 2, 3$ denotes the Cartesian coordinates x, y, and z, respectively. The remaining quantities are defined as follows. The quantity $\mathbf{U} = (U_1, U_2, U_3) = (u,v,w)$ is the velocity field at a given point, and $\mathbf{x} = (x_1, x_2, x_3) = (x,y,z)$ is the Cartesian coordinate of that point. The quantity V_B is the speed of the beam, moving in the direction of increasing x, and δ_{1j} is the Kronecker delta function. The quantity P is the pressure at a given point, and T is the temperature. The quantities B_j are the body force terms due to the buoyancy force and are given by:

$$\mathbf{B} = -\rho\beta\mathbf{g}(T - T_M) \quad [4]$$

where T_M is the melting temperature of the metal. The quantity $\mu(T)$ is the coefficient of viscosity as a function of temperature and is approximated by the expression:

$$\mu(T) = \mu_s[1 - u_s(T - T_M)] + \mu_l \quad [5]$$

where μ_s is some very large number representing an infinite viscosity in a solid and $u_s(T - T_M)$ is a unit step function such that:

$$u_s(T - T_M) = 0 \text{ if } T \leq T_M, 1 \text{ otherwise} \quad [6]$$

For the sample calculations shown in this article, physical quantities approximating those of iron or steel are adopted for the model system. Therefore, this model is not representative of a specific system, but rather of a general prototype iron-steel system. These quantities and others that are associated with numerical discretization and model specification are given below and in Appendix C. The heat capacity in J/kg · K is given by the expression:[10]

$$C_p(T) = \begin{cases} 1.117 \times 10^6(1010 - T)^{-2} + 12\,622(1010 - T)^{-1} \\ \quad + 0.3485T + 355.6 \quad \text{if } T < 1000\ K \\ 1.225 \times 10^8(T - 990)^{-4} + 0.1381T + 585.7 \text{ otherwise} \end{cases} \quad [7]$$

This function has been adopted for $C_p(T)$ because of its qualitative behavior. In the present study, no quantitative significance is given to the values of $C_p(T)$ for the range of temperature in the neighborhood of $T = 1000$ K (727 °C), where it changes considerably with T. The function given by Eq 7 provides a representation of exothermic energy release for the purpose of examining the general influence of reactions that can occur in the workpiece during welding. The conductivity in W/m · K as a function of temperature in degrees Kelvin is given by the following expression:

$$k(T) = \begin{cases} 70.4138 - 0.038125T & \text{if } T < 1073.15 \\ 41.0 & \text{if } 1073.15 \leq T < 1763.15 \\ -862.5375 + 0.5125T & \text{if } 1763.15 \leq T < 1803.15 \\ 61.5 & \text{if } 1803.15 \leq T < 2800.15 \\ 865.34829 - 0.28707T & \text{if } 2800.15 \leq T < 3014.15 \end{cases} \quad [8]$$

In Eq 1 and 2, the influence of convection is represented by two terms, i.e., a term containing **U** and one containing V_B. This representation follows because the flow field associated with the convection terms in both the energy and momentum transport equations, i.e., Eq 1 and 2, is defined with respect to an origin that is fixed in the workpiece. The component of the flow field parallel to the direction of the motion of the beam is therefore $\rho(u + V_B)$; however, the dependent variables of the momentum transfer equations (u,v,w) are the velocities relative to an origin that is stationary with respect to the beam. The weighting coefficients for the discretization of Eq 2, as defined by the SIMPLE algorithm,[9] are modified to take this representation into account.

2.2 *Effects Entering the Model Through the Boundary Conditions*

The effect of surface tension enters the model via the boundary conditions on the momentum transport equations. This is described in the next section. The deposition of power from the beam enters the model via time-dependent boundary conditions on the energy transfer equation (Eq 1). At each timestep, an isothermal region of the workpiece at the temperature of vaporization is specified according to the relation:

$$T_B = \min[T_G, Q_1(z)Q_2(x,y,t)] \quad [9]$$

where

$$Q_1(z) = Q_0 \exp(-\beta_b z) \quad [10]$$

$$Q_2(x,y,t) = \exp\left[-\left(\frac{3}{R_b^2}\right)[(x - V_B t)^2 + y^2]\right] \quad [11]$$

and T_G is the temperature of vaporization. The quantity of Q_2 is a distribution that specifies the deposition of power on the surface of the keyhole relative to the beam center. The function Q_1 specifies the layer depth for energy deposition on the surface. All node points with $T = T_G$ are defined as the union of interior and boundary points of the keyhole.

At the keyhole liquid/vapor interface, the boundary conditions on the momentum transfer equations are those of a no-slip boundary. That is, the component of the velocity, in the reference frame of the workpiece, normal to the interface is zero:

$$\mathbf{U} \cdot \hat{\mathbf{n}} + \mathbf{V_B} \cdot \hat{\mathbf{n}} = 0 \quad [12]$$

where $\hat{\mathbf{n}}$ is the unit normal to the keyhole liquid/vapor interface and $\mathbf{V_B}$ is the velocity of the beam with respect to the workpiece and is in the x-direction. Another boundary on the molten region is defined by the solid/liquid interface. The boundary condition on this boundary is specified in the model according to the equation:

$$U_j = -\delta_{1j} V_B \text{ if } T < T_M \quad [13]$$

Note that according to this specification the set of all nodes having temperature values less than T_M includes both boundary and exterior points of the melt pool.

3. Boundary Conditions on the Faces of the Sample

In this section, the boundary conditions on each face of the sample (see Fig. 1) are specified with respect to temperature and velocity. Boundary conditions on the xy face at $z = 0$ are

$$\frac{\partial T}{\partial z} = 0 \qquad [14a]$$

$$\mu\frac{\partial u}{\partial z} = -\frac{\partial \gamma}{\partial T}\frac{\partial T}{\partial x} \text{ and } \mu\frac{\partial v}{\partial z} = -\frac{\partial \gamma}{\partial T}\frac{\partial T}{\partial y} \text{ if } T_M \le T \le T_G \qquad [14b]$$

$$u = -V_B \text{ and } v = 0 \text{ otherwise} \qquad [14c]$$

and

$$w = 0 \qquad [14d]$$

The quantity $\partial\gamma/\partial T$ is the thermal coefficient of surface tension. Boundary conditions on the xy face at $z = L_z$ are

$$\frac{\partial T}{\partial z} = 0 \qquad [15a]$$

$$\mu\frac{\partial u}{\partial z} = -\frac{\partial \gamma}{\partial T}\frac{\partial T}{\partial x} \text{ and } \mu\frac{\partial v}{\partial z} = -\frac{\partial \gamma}{\partial T}\frac{\partial T}{\partial y} \text{ if } T_M \le T \le T_G \qquad [15b]$$

$$u = -V_B \text{ and } v = 0 \text{ otherwise} \qquad [15c]$$

and

$$w = 0 \qquad [15d]$$

Boundary conditions on the xz face at $y = 0$ are

$$\frac{\partial T}{\partial y} = 0 \qquad [16a]$$

$$\frac{\partial u}{\partial y} = 0 \quad v = 0 \text{ and } \frac{\partial w}{\partial y} = 0 \qquad [16b]$$

Boundary conditions on the xz face at $y = L_y$ and at time $t + \Delta t$ are

$$\frac{\partial T}{\partial y} = 0 \qquad [17a]$$

if L_y coincides with the physical edge of the workpiece, or

$$T(t + \Delta t) = T(t) + \left(\frac{k\Delta t}{\rho C_p}\right)\frac{d^2T}{dy^2} \qquad [17b]$$

if L_y does not coincide with the physical edge of the workpiece.

$$u = -V_B \quad v = 0 \text{ and } w = 0 \qquad [17c]$$

Boundary conditions on the yz face at $x = 0$ and at time $t + \Delta t$ are

$$T(t + \Delta t) = T(t) + \left(\frac{k\Delta t}{\rho C_p}\right)\frac{d^2T}{dx^2} \qquad [18a]$$

where $x = 0$ does not coincide with the physical edge of the workpiece.

$$u = -V_B \quad v = 0 \text{ and } w = 0 \qquad [18b]$$

Boundary conditions on the yz face at $x = L_x$ are

$$T = T_A \qquad [19a]$$

$$u = -V_B \quad v = 0 \text{ and } w = 0 \qquad [19b]$$

It is important to note that the boundary conditions on the system boundaries at face xz at $y = L_y$, face yz at $x = 0$, and face yz at $x = L_x$ are physically consistent only if solidification has occurred in the neighborhood of these boundaries; that is, only if the temperature at grid points in the neighborhood of these boundaries is less than T_M so that $u = -V_B$. Additionally, the rate of energy transfer and the positioning of the beam in the model system should not be such that the boundary conditions given by Eq 19a and 19b are invalid. That is, the system parameters should always be such that the values of the temperature in the neighborhood of the yz face at $x = L_x$ are T_A.

4. Computational Issues

4.1 *Formulation of the SIMPLE Algorithm for Modeling Welding Processes*

A derivation of the discretization equations that define the SIMPLE algorithm are given elsewhere.[9] The current model uses a formulation of this algorithm that is structured for the type of modeling considered here. Thus, the formulation is structured to provide an accurate coupling between energy transfer and the stirring action of the keyhole boundary. Furthermore, this formulation provides an explicit representation of this coupling and of the dependence of energy transfer on keyhole stirring. This formulation is defined by:

$$\varphi_p = \zeta\left[\sum_{k=1}^{6} a_k\varphi_k + \frac{\rho\Delta l^3\,\varphi_p^0}{\Delta t} + S_p\right] \qquad [20]$$

where

$$\zeta = \left[\sum_{k=1}^{6} a_k + \frac{\rho\Delta l^3}{\Delta t}\right]^{-1} \qquad [21]$$

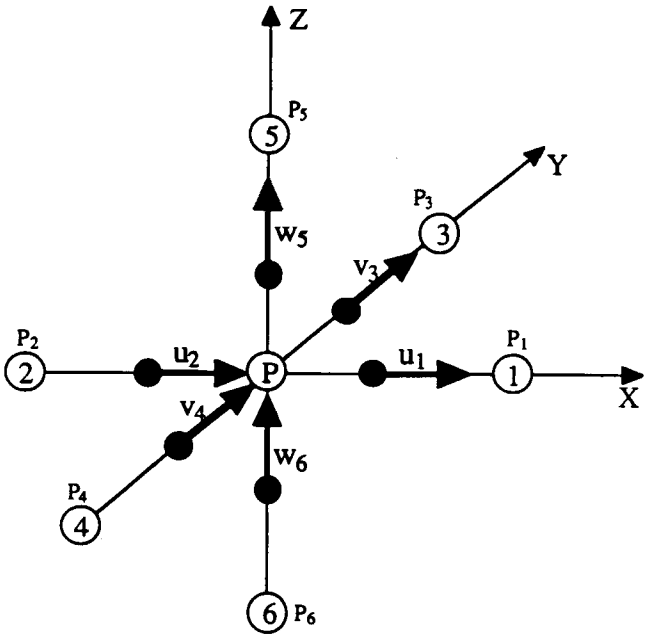

Fig. 2 Indexing scheme for node neighbors and associated dynamical quantities.

The weighting coefficients a_k are given by

$$a_k = \Gamma_k \Delta l A(|P_e(k)|) + \max[(-1)^k \rho \Delta l^2 (V_k + (\delta_{1k} + \delta_{2k}) V_B), 0] \quad [22]$$

where

$$P_e(k) = \rho[V_k + (\delta_{1k} + \delta_{2k}) V_B] \Delta l \, \Gamma_k^{-1} \quad [23]$$

and

$$A(|P_e(k)|) = \max[0, (1.0 - 0.1|P_e(k)|)^5] \quad [24]$$

The integer variable k specifies with which of the six nearest neighbor nodes of node p a given quantity is to be associated. This is described schematically in Fig. 2. In Eq 20 to 24, if the field quantity φ is the temperature T, then $\Gamma = k(T)$ and $S_p = 0$. If the field quantity φ is u, v, or w, then $\Gamma = \mu(T)$ and $S_p = (\partial P/\partial x_j)\Delta l^3 + B_j$. The quantity φ_p^0 is the value of φ_p at the previous timestep. The weighting coefficients a_k follow by deriving the discretization equations of SIMPLE from the model system defined by Eq 1 and 2 with the condition of fixed or uniform separation between grid points. The significance of this condition in the current formulation is discussed below. The quantity V_k is given by:

$$V_k = \delta_{1k} u_1 + \delta_{2k} u_2 + \delta_{3k} v_3 + \delta_{4k} v_4 + \delta_{5k} w_5 + \delta_{6k} w_6 \quad [25]$$

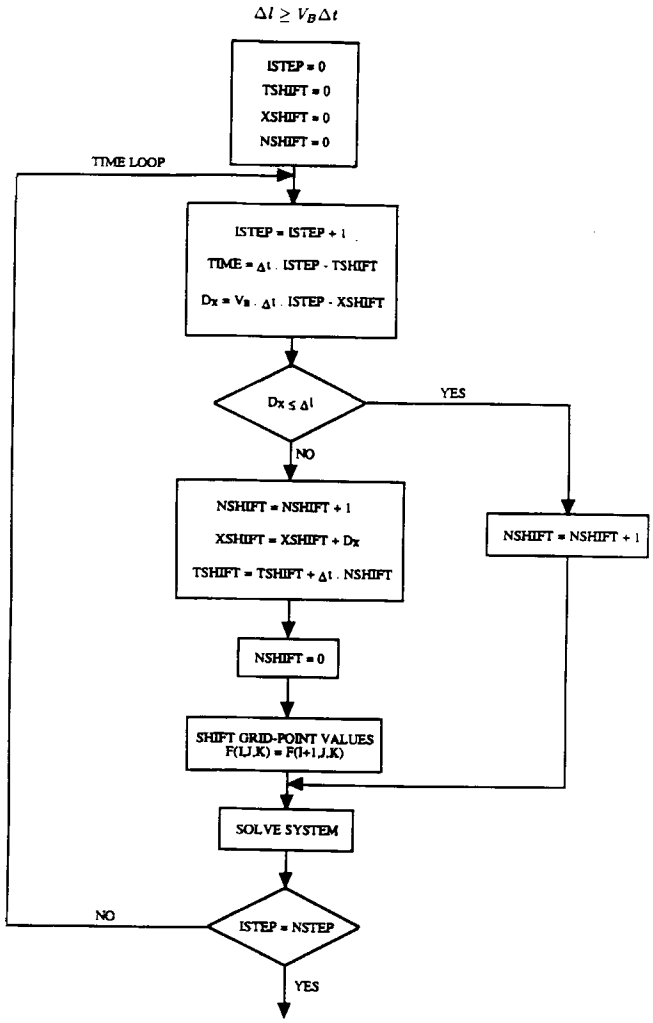

Fig. 3 Procedure for shifting grid relative to beam center for the case $\Delta l \geq V_B \Delta t$.

and is the component of the velocity orthogonal to the faces of a rectangular volume centered at node p (see Fig. 2).

The significant features of the above formulation of the SIMPLE algorithm for modeling the coupling of energy transfer in the weld pool to keyhole stirring are embodied in the weighting coefficients defined by Eq 22 and 23. The weighting factor A, whose value is between 0 and 1, is a function of the Peclet number $P_e(k)$ and varies according to the influence of convective energy transfer relative to energy transfer by conduction. The coefficients a_k are constructed so that there is an accurate weighting of the influence due to stirring. The stirring action of the keyhole, unlike other mechanisms for driving fluid flow, is the result of coupling between the motion of the molten pool and the geometric constraint imposed by the keyhole boundary.

The rate of energy input into the system is a function of the beam profile parameters defined in Eq 10 and 11 and the beam speed V_B. The energy input is effected via the time-dependent boundary conditions associated with the keyhole vapor/liquid

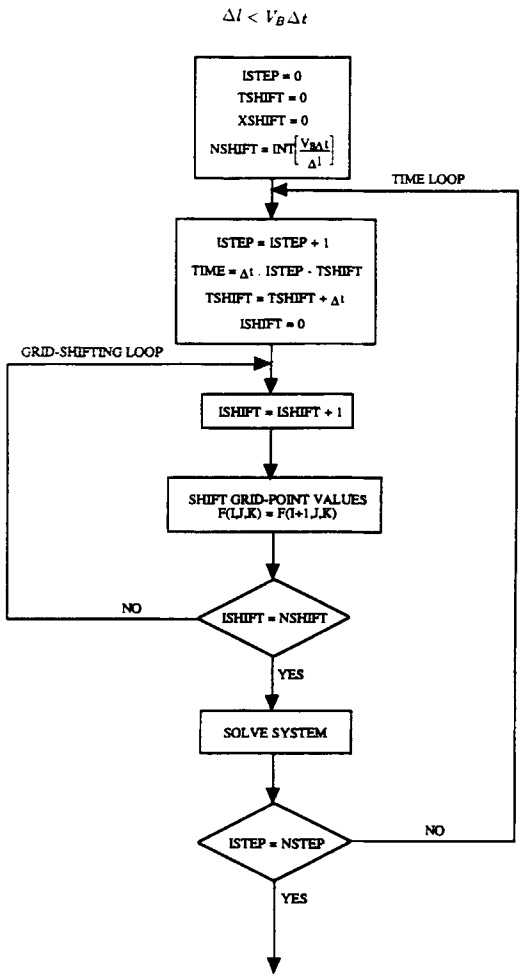

Fig. 4 Procedure for shifting grid relative to beam center for the case $\Delta l < V_B \Delta t$.

interface. The time-dependence of the keyhole boundary conditions results from the shifting of the grid relative to the beam center. The procedure for shifting the grid depends on the size of the distance between nodes Δl relative to the quantity $V_B \Delta t$, where Δt is the timestep of integration. These procedures are illustrated in Fig. 3 and 4.

4.2 *Convergence Criteria for Iterative Schemes*

The system of discretization equations is solved iteratively until the convergence criterion

$$\max \left| \varepsilon_{ijk}^n \right| < \varepsilon_{\max} \qquad [26]$$

is satisfied. The quantity $\varepsilon_{\max}$ is the maximum error tolerance and

$$\varepsilon_{ijk}^n = \left| \varphi_{ijk}^n - \varphi_{ijk}^{n-1} \right| \left| \varphi_{ijk}^n \right|^{-1} \qquad [27]$$

In Eq 26 and 27, the subscript denotes the grid point and the superscripts the iteration. Successive iterations consist of underrelaxation according to

$$\varphi_p^n = \varphi_p^{n-1} + \alpha \left(\zeta \left[\sum_{k=1}^{6} a_k \varphi_k^{n*} + \frac{\rho \Delta l^3 \varphi_p^0}{\Delta t} + S_p \right] - \varphi_p^{n-1} \right) \qquad [28]$$

where the superscript n^* denotes the most current iterate, which can be either n or $n-1$, and the relaxation coefficient α is less than 1. In the case of fluid velocity, the authors have defined a relative error scaled by the beam velocity, i.e.,

$$\varepsilon_{ijk}^n = \begin{cases} \left| \varphi_{ijk}^n - \varphi_{ijk}^{n-1} \right| \left| \varphi_{ijk}^n \right|^{-1} & \text{if } \varphi = u \\ \left| \varphi_{ijk}^n - \varphi_{ijk}^{n-1} \right| \left(\left| \varphi_{ijk}^n \right| + V_B \right)^{-1} & \text{otherwise} \end{cases} \qquad [29]$$

Once convergence is achieved for a particular region of the workpiece, i.e., Eq 26 is satisfied for a sufficiently large and connected set of nodes and for a sufficiently long time interval, the values of the dependent variables at the node points within this region, φ_{ijk}, need no longer be changed, and the iteration on these variables stops. Thus, the work per iteration decreases as the iteration progresses. This follows because the weighting coefficients a_k are computed from the converged values of the previous set of iterations.

4.3 *Evaluation of No-Slip Boundary Conditions*

The solution of the no-slip boundary condition is of the form:

$$\mathbf{U}_{ijk} = P(\hat{\mathbf{n}})(\mathbf{U}_{lmn} + \mathbf{V_B}) \qquad [30]$$

where $\hat{\mathbf{n}}$ is the unit normal to the keyhole liquid/vapor surface at the node ijk, which is a boundary point. The quantity $\mathbf{U}_{lmn}$ is the velocity at a node lmn exterior and nearest to the boundary and along $\hat{\mathbf{n}}$ (see Fig. 5), and $P(\hat{\mathbf{n}})$ is the projection operator that forms a vector orthogonal to $\hat{\mathbf{n}}$. The nodes $\{lmn\}$ are the set of all exterior points that are most adjacent to the boundary. For $\mathbf{U}_{ijk}$ to be computed, the node ijk must be identified as a boundary point, the node lmn must be identified, and $\hat{n}$ must be computed.

To identify a given node as a boundary point, the temperature at each node and its six adjacent nodes is examined. The node ijk is identified via a search algorithm that takes advantage of the shape of the keyhole. Because the radius of the keyhole cannot exceed the radius of the laser beam (R_b in Eq 11), the number of comparisons required to identify all boundary points is bounded above by $7n_{\text{beam}}^2 n_z$ where n_{beam} corresponds to the number of nodes that the beam surface has enclosed in the z-direction (see Fig. 5).

Once the nodes ijk and lmn are determined, the normal is given by

$$\mathbf{n} = \mathbf{x}_{lmn} - \mathbf{x}_{ijk} \qquad [31]$$

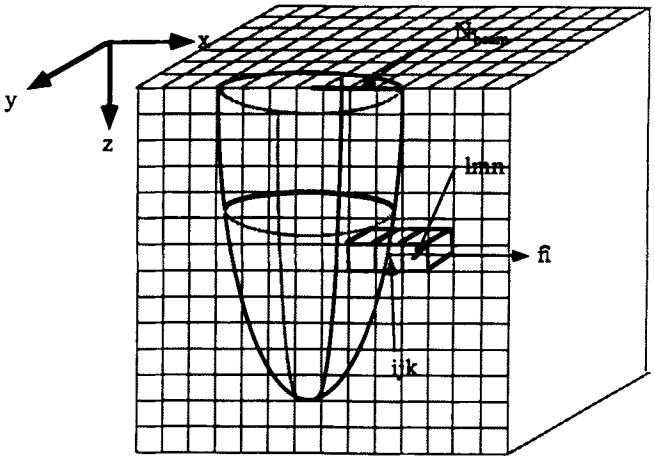

Fig. 5 Schematic of model system showing nodes used for calculating no-slip boundary conditions.

and the projection operator $P(\hat{\mathbf{n}})$ is given by

$$P(\hat{\mathbf{n}}) = I - \frac{\mathbf{n}\mathbf{n}^T}{\mathbf{n}^T\mathbf{n}^T} \quad [32]$$

This form of the operator eliminates the need to compute the Euclidian norm of **n** and therefore eliminates a computationally costly square root calculation.

4.4 *Calculation of Pressure Field*

An expression for iteratively calculating a correction to the pressure is presented such that the resulting field is consistent with both the momentum transport and continuity equations. This expression represents a further modification of the SIMPLE algorithm and is based on a second-order central difference of the pressure field. In addition, this expression is not defined in terms of shifted-grid quantities.

At each iteration, it is desired to calculate a discrete pressure field P_p such that $U_{p,i}$, where p designates the node point, satisfies Eq 1, as well as the expression:

$$\sum_{i=1}^{3} \frac{\partial U_{i,p}}{\partial x_i} = 0 \quad [33]$$

It can be shown that, if $U^*_{i,p}$ satisfies Eq 20 for the pressure field P^*_p, then for a pressure field $P_p = P^*_p + P'_p$, where P'_p is the pressure correction, the corrected velocity field is given by

$$U_{i,p} = U^*_{i,p} + \zeta\left(\frac{\partial P'_p}{\partial x_i}\right)\Delta l^3 \quad [34]$$

The expression for the pressure correction that is derived in Appendix A is given by

$$P'_p = 1/6\sum_{k=1}^{6} P'_k + \frac{B}{6\Delta l} \quad [35]$$

where

$$B = \zeta^{-1}\sum_{i=1}^{3} \frac{\partial U^*_{i,p}}{\partial x_i} \quad [36]$$

and the method for numerically calculating the derivatives, $\partial U^*_{i,p}/\partial x_i$, is arbitrary and not a formal part of the derivation of Eq 35 (see Appendix A).

4.5 *Discussion of Computational Issues*

The present study concerns two issues. One is the characterization of the general influence on energy transfer due to the physical conditions in the neighborhood of the keyhole vapor/liquid interface. The other is the development of a prototype model system of deep penetration welding that is easily extendable to more detailed and quantitative analysis and that eventually can be realized as a practical tool for process modeling of different types of deep penetration welding processes. The authors have therefore adopted a discrete formulation of the model system, based on SIMPLE, that emphasizes its convenience and adaptability. In this section, the important features of that formulation are described that should be relevant *in practice* to achieving a reasonable combination of accuracy, efficiency, and model flexibility. A rigorous evaluation of the formulation in terms of overall optimality has not been considered and remains an open issue for further investigation. However, experience gained using this model and a preliminary examination of its underlying mathematical properties suggest that the formulation is both a convenient and reasonably tractable approach for process modeling involving complex or unsteady keyhole structures.

The important features of the formulation are reviewed and contrasted to the original formulation of SIMPLE. A discretization scheme has been adopted that is based on a uniform or fixed grid separation, i.e., Δl in Eq 20 through 23. The discretization scheme of Patankar and co-workers[9] is based on a grid whose separation of nodes is locally variable and is therefore in general nonuniform. This aspect of the original formulation is important for local grid refinement where higher levels of resolution are required. Another feature that was adopted in the formulation is that of a *single* grid system. The original formulation used a combination of grids, i.e., a *main* grid and a *shifted* grid. This feature of the original formulation contributes to both its efficiency and accuracy because it permits the calculation of gradients of the different quantities, i.e., T, U_j, and P, to be at the same level of accuracy and computational cost. The reasons for not adopting this feature are discussed below. Because this formulation is based on a single grid, it is necessary to adopt a consistent pressure correction equation. Therefore, the authors derived a pressure correction equation that was based on a single grid system. This derivation does not include as part of its formal development any specific finite difference approxima-

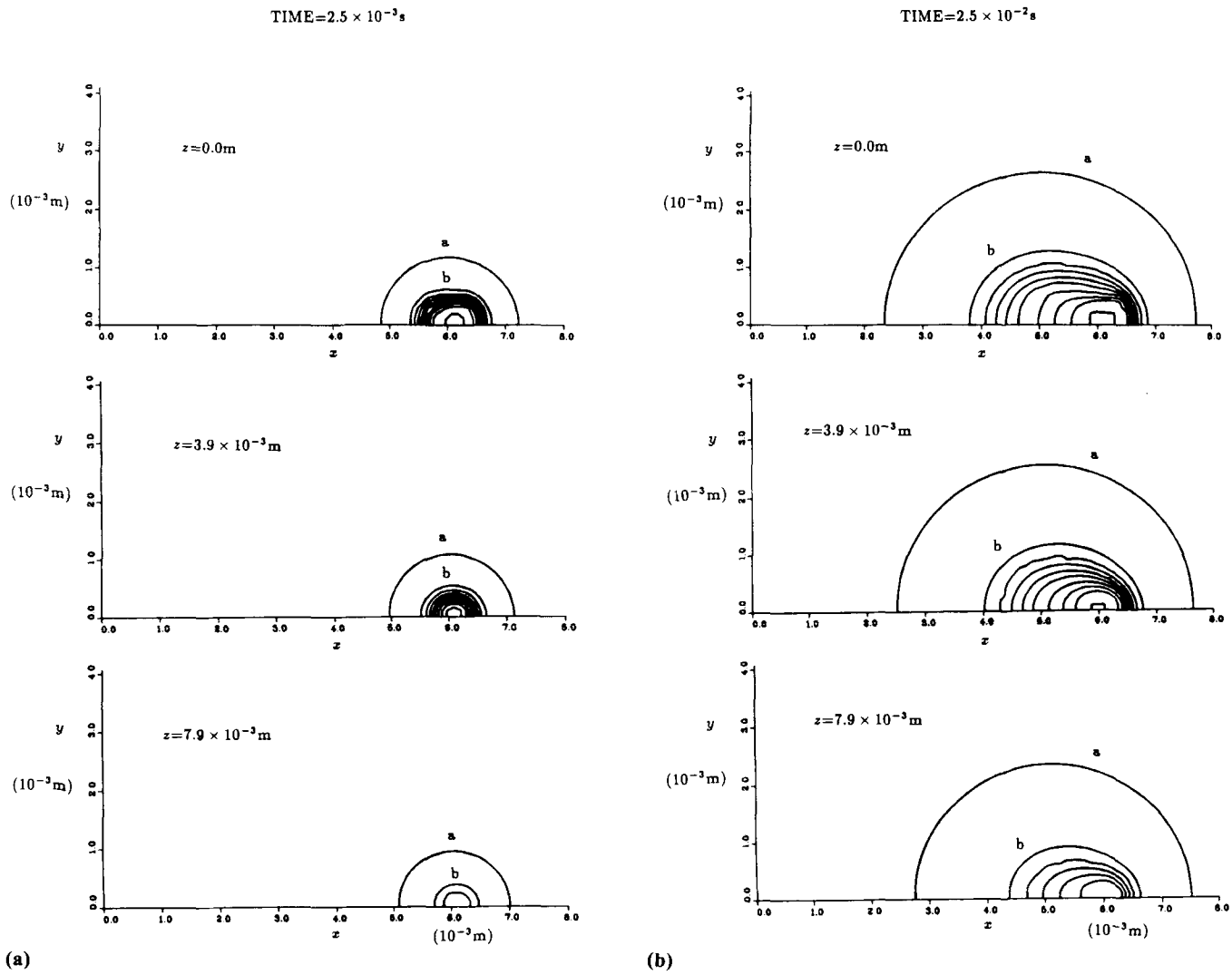

Fig. 6 Unsteady evolution of model system to steady state for weld pool. Model system includes surface tension and buoyancy. The temperatures of the isotherms are (a) 35 °C, (b) 335 °C, (c) 635 °C, (d) 935 °C, (e) 1235 °C, and (f) 1535 °C. In cases where isotherms are not labeled, temperatures of isotherms are assigned as follows. The outermost isotherm is at 35 °C. Isotherms that are successively closer to the keyhole are at temperatures in the sequence 335, 635, 935, 1235, 1535, 1835, 2135, and 2435 °C and T_G.

(continued)

tion of the velocity gradients (see Eq 36). However, it does include a physically reasonable condition on the character of the local variation of the pressure field at the boundaries, i.e., Eq A6 in Appendix A. It is important to note that the use of a single, uniformly spaced grid requires in general a higher computational cost for calculating the quantities $\partial P/\partial x_j$ and $\partial U^*_{j,p}/\partial x_j$ relative to the computational cost of achieving comparable accuracy with a shifted grid system. The reason for adopting a formulation of SIMPLE that is based on a single, uniformly spaced grid is that the mathematical properties of this algorithm permit it to be combined with the method of embedded meshes[11] for adaptive local grid refinement. In general, because SIMPLE is an implicit formulation, grid spacing is independent of the timestep size and can be varied locally to achieve a desired resolution. Thus, the method of embedded meshes combined with SIMPLE is mathematically equivalent to the original formulation of SIMPLE, which is based on a locally variable *global* grid. However, the embedded mesh method is found to be highly flexible for locally adapting grid resolution according to the details of flow structures that can occur in deep penetration welding problems. Reference 11 discusses the general features of the embedded mesh method.

5. Case Study of Factors Influencing the Shape of the Weld Pool

For the prototype iron-steel system considered here, a case study of the sensitivity of the shape of the molten pool with respect to several general physical aspects of deep penetration welding processes is presented. The sensitivity of the shape of the melt pool with respect to keyhole stirring, surface-tension

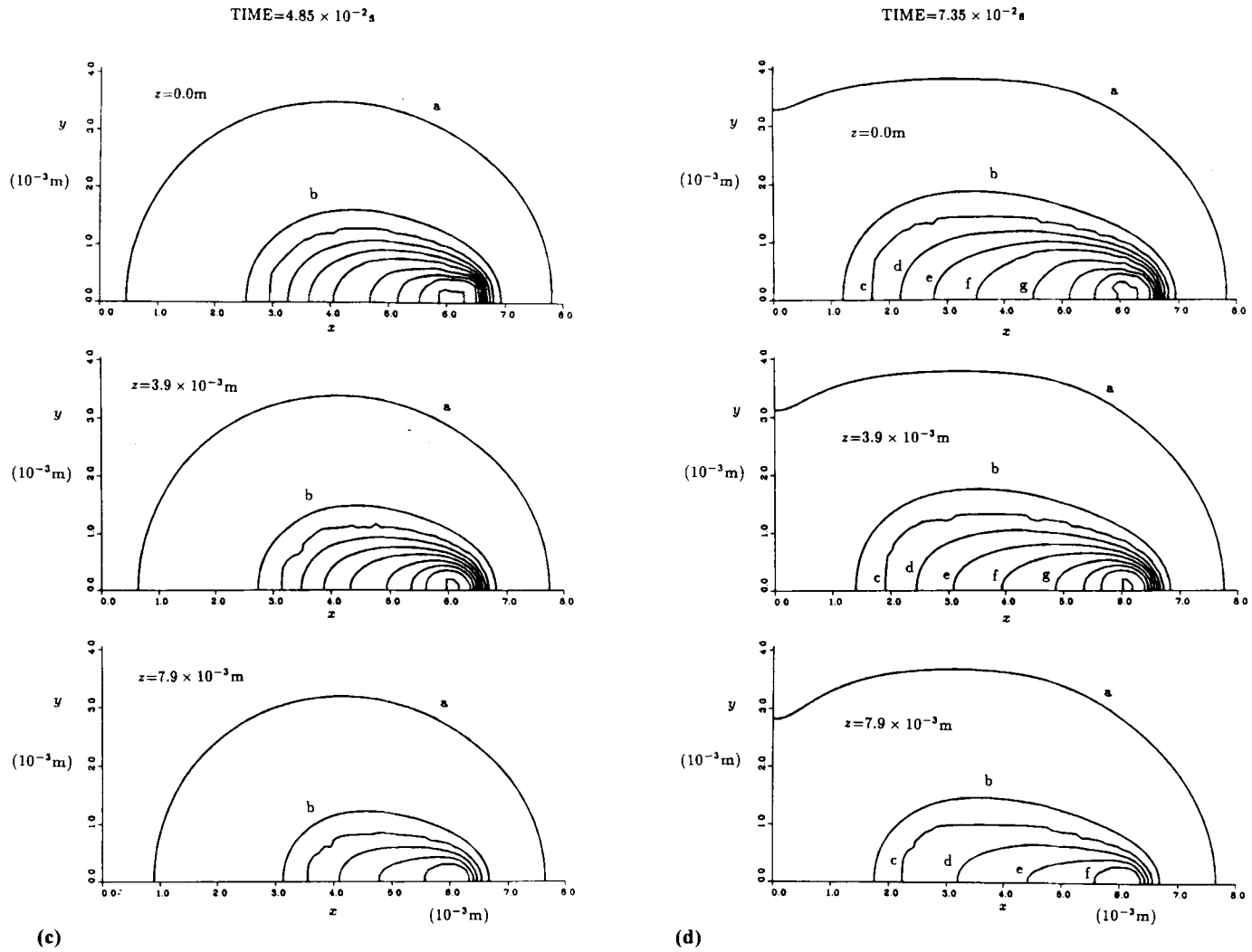

Fig. 6 Unsteady evolution of model system to steady state for weld pool. Model system includes surface tension and buoyancy. The temperatures of the isotherms are (a) 35 °C, (b) 335 °C, (c) 635 °C, (d) 935 °C, (e) 1235 °C, and (f) 1535 °C. In cases where isotherms are not labeled, temperatures of isotherms are assigned as follows. The outermost isotherm is at 35 °C. Isotherms that are successively closer to the keyhole are at temperatures in the sequence 335, 635, 935, 1235, 1535, 1835, 2135, and 2435 °C and T_G.

(continued)

driven flow, and the rate of energy transfer in the solid were considered. An analysis of the relative influence of surface tension is important in that surface tension has been shown to be a significant driving force for fluid flow in welding processes where energy deposition occurs on the surface of the workpiece. An analysis of the relative influence of energy transfer in the solid is important because it provides a basis for increasing both the accuracy and efficiency of process simulations. This is explained below.

Figures 6(a) through (g) show the unsteady evolution of the model system to a steady state of the three-dimensional weld pool. The isotherm labeled "f" in these figures designates approximately the solid/liquid boundary. This simulation uses a model system that includes buoyancy and surface tension. In addition, for this simulation the authors have imposed the condition of zero conductivity at the boundaries for the purpose of maintaining unsteady energy transfer in the solid. That is, the boundary conditions are such that the system continuously heats up at the boundaries and cannot achieve a global steady state for conduction in the solid. Figure 7 shows a state of the model system that is calculated via a simulation that is the same as that described by Fig. 6, except that the model system does not include surface tension. Figure 6(g) and 7 show system states corresponding to the same simulation time and exhibit weld pool shapes corresponding to steady states of the flow field in the weld pool. A comparison of Fig. 6(g) and 7 shows that the influence of surface tension is small relative to the stirring action of the keyhole. There is a relatively small difference between the weld pool shapes shown in Fig. 6(g) and 7. This is consistent with the highly localized character of the energy source. The onset of any fluid structures due to surface tension, e.g., Marangoni flow structures, are quickly damped because of

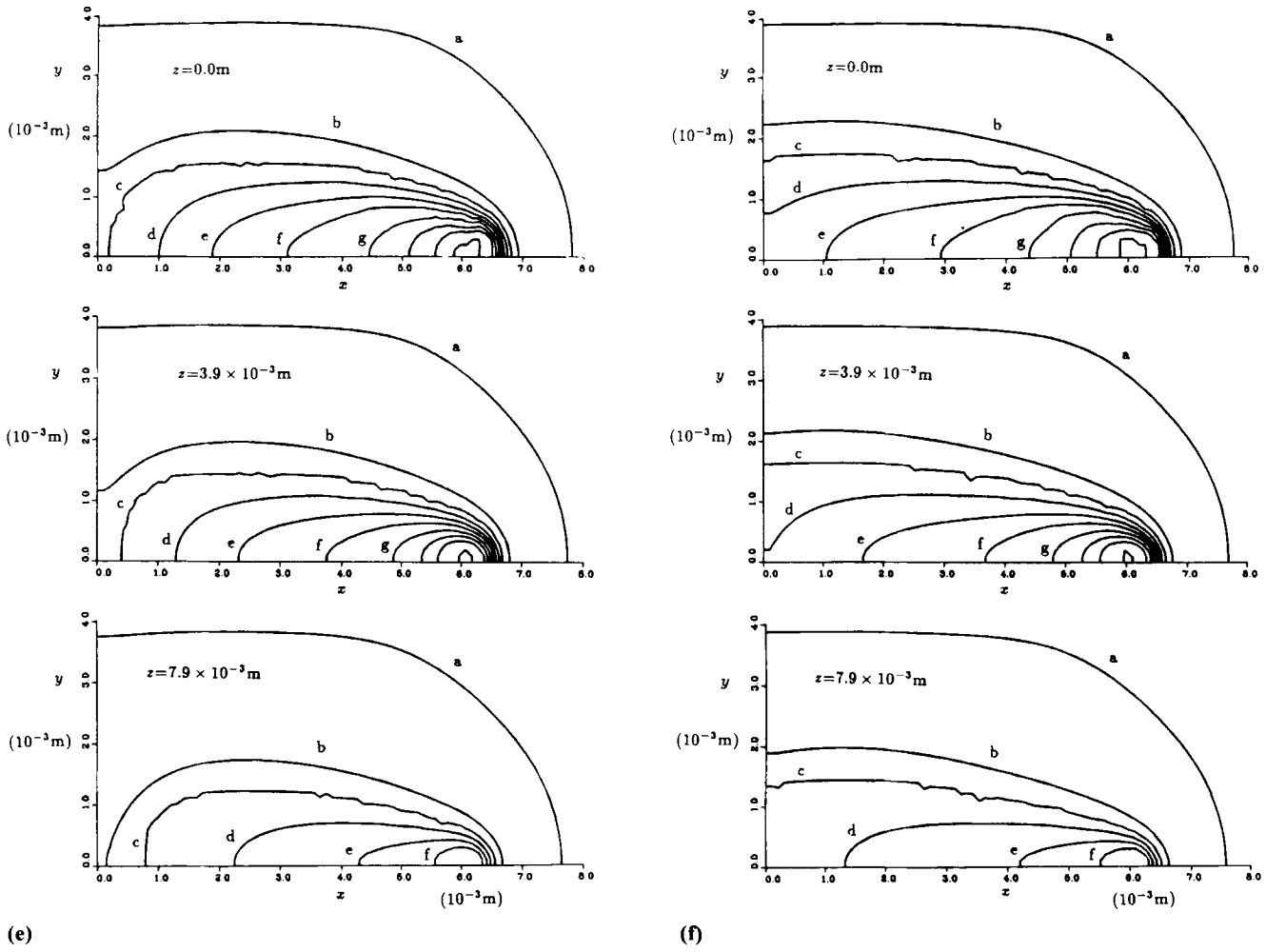

Fig. 6 Unsteady evolution of model system to steady state for weld pool. Model system includes surface tension and buoyancy. The temperatures of the isotherms are (a) 35 °C, (b) 335 °C, (c) 635 °C, (d) 935 °C, (e) 1235 °C, and (f) 1535 °C. In cases where isotherms are not labeled, temperatures of isotherms are assigned as follows. The outermost isotherm is at 35 °C. Isotherms that are successively closer to the keyhole are at temperatures in the sequence 335, 635, 935, 1235, 1535, 1835, 2135, and 2435 °C and T_G.

(continued)

the relatively rapid onset of solidification in the trailing pool. Furthermore, this result supports experimental observations that in deep penetration welding processes keyhole stirring is the dominant influence on fluid flow in the weld pool. Although the current model considers an energy source of specific character, i.e., a continuous-beam energy source with a specific spatial distribution, the dominant influence of keyhole stirring demonstrated in this case study should represent a general characteristic of the deep penetration welding processes. This follows because, for deep penetration welding, a large fraction of the weld pool is always in close proximity to the keyhole and is therefore influenced primarily by stirring. The dominant influence of stirring is due to the spatially local character of the beam source and is not due to any particular temporal behavior or shape of the keyhole vapor/liquid surface.

As is shown in Fig. 6(a) through (g), after a period of time, the molten pool achieves a steady-state shape that is insensitive to the unsteady energy transfer at points in the solid that are relatively removed from the solid/liquid boundary. This property of the system implies that one can extend the same approach used here for modeling the keyhole vapor/liquid interface to modeling the liquid/solid interface. As with the keyhole, however, this approach assumes a time average of local changes in shape of the liquid/solid surface. The steady-state liquid/solid surface can be adopted as a moving surface, upon which energy is deposited. That is, a boundary whose temperature is kept constant by continuously adding energy to the system. In this case, however, energy deposition is due to the combined system of keyhole and melt pool. As with the keyhole, this approach eliminates the need for calculating

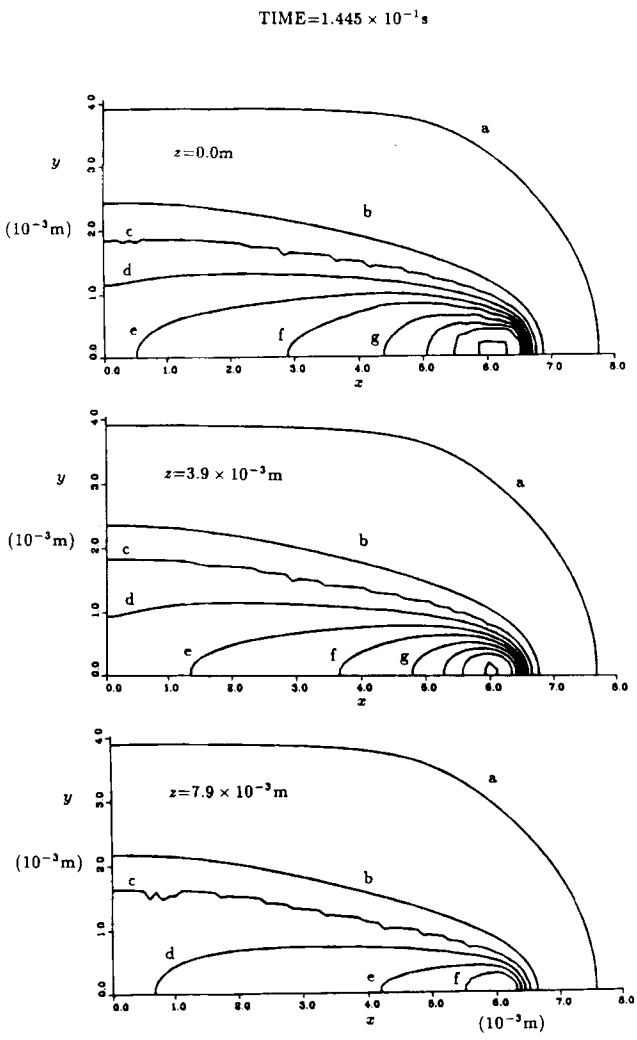

(g)

Fig. 6 Unsteady evolution of model system to steady state for weld pool. Model system includes surface tension and buoyancy. The temperatures of the isotherms are (a) 35 °C, (b) 335 °C, (c) 635 °C, (d) 935 °C, (e) 1235 °C, and (f) 1535 °C. In cases where isotherms are not labeled, temperatures of isotherms are assigned as follows. The outermost isotherm is at 35 °C. Isotherms that are successively closer to the keyhole are at temperatures in the sequence 335, 635, 935, 1235, 1535, 1835, 2135, and 2435 °C and T_G.

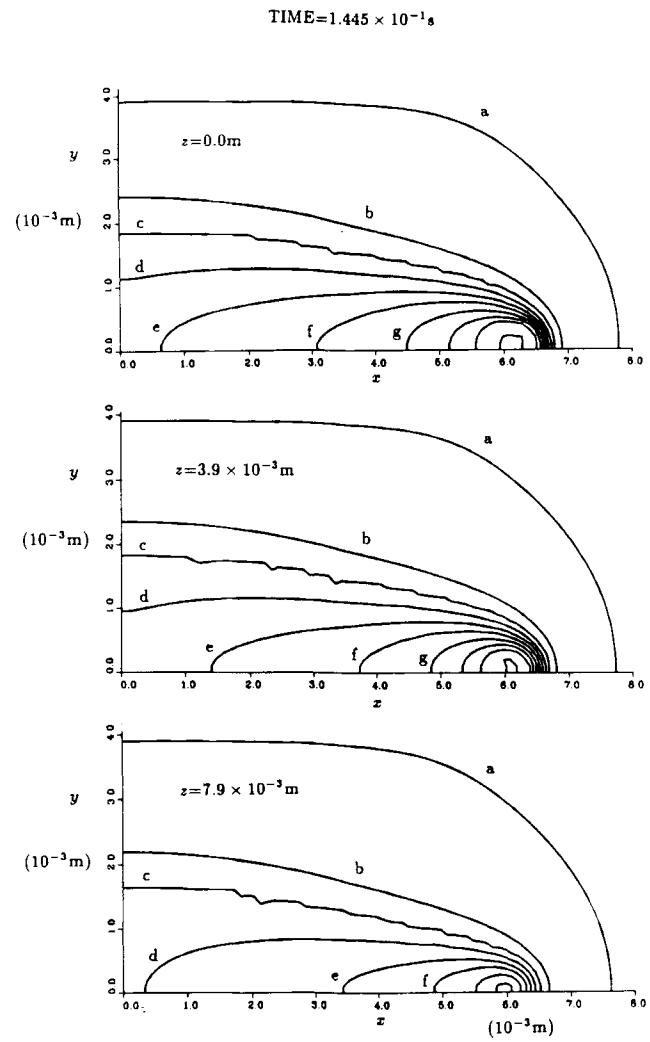

Fig. 7 Steady state of weld pool for model system without surface tension. This system state and that shown in Fig. 6(g) are at the same simulation time. The temperatures of isotherms are assigned as in Fig. 6.

structures outside the boundary and thus contributes significantly to increased efficiency and problem tractability. For example, thermal cycles can be calculated for inhomogeneous systems or systems containing inclusions that do not interact with the melt pool. Furthermore, increased accuracy and efficiency can be achieved by first modeling the evolution of the melt pool to steady state using a model system whose boundaries are close to the liquid/solid interface. The calculated weld pool surface can then be adopted as a moving boundary in a model system that is only in a solid phase. An explanation of the mathematical basis for extending the current approach for modeling the keyhole boundary to modeling the liquid/surface boundary follows from an examination of the transition of this model system to a steady state in both the temperature and fluid velocity field. This simulation demonstrates the weak coupling between processes occurring in different parts of the workpiece during the overall welding process.

6. Unsteady Process and Evolution of System to Steady State

Figures 8(a) through (f) show the unsteady evolution of the model system to a steady state for both the temperature and fluid velocity field. The initial state for this simulation is that shown in Fig. 6(g). For this simulation, the heat flux out/flow boundary conditions given by Eq 17b and 18a have been applied to the system, allowing the system to achieve a steady

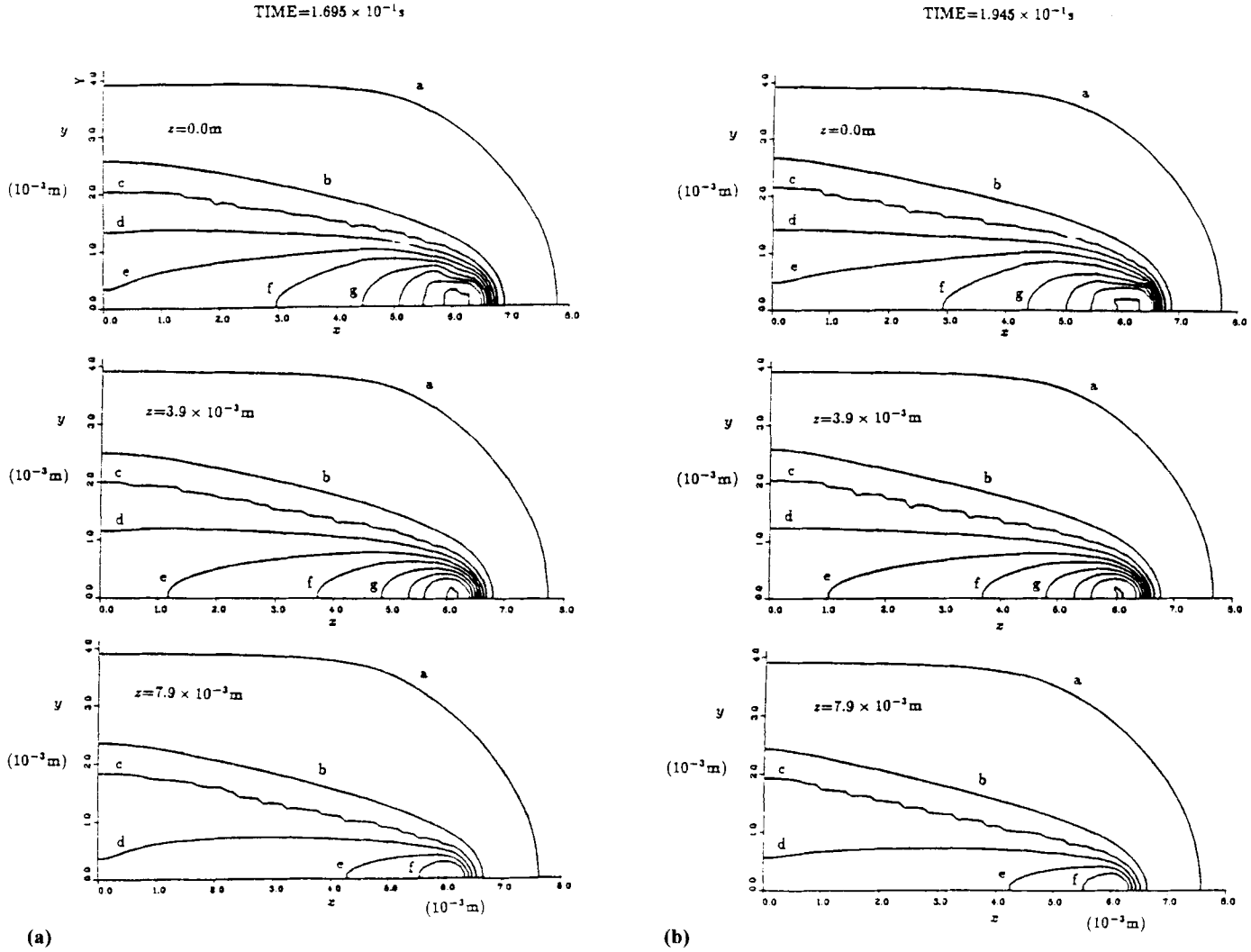

Fig. 8 Unsteady evolution of model system to steady state for both temperature and fluid velocity field. The temperatures of isotherms are assigned as in Fig. 6.

(continued)

state for the temperature field. A comparison of the system states (Fig. 6a to 6g and 8a to 8f) shows several general characteristics of these simulations. First, the shape of the weld pool, after having reached a steady state, is independent of the heat flux out/flow boundary conditions. Second, the unsteady evolution of the temperature field in the solid, for a large fraction of the workpiece in the vicinity of the melt pool, is not influenced by the rear and side boundary conditions. Third, although the rear boundary conditions do not influence the temperature field in the vicinity of the melt pool, they do influence the temperature field in the vicinity of the rear boundary. These general characteristics follow because both the fluid velocity field in the melt pool and the temperature field in the vicinity of the melt pool are influenced by system conditions upstream, i.e., these fields have parabolic spatial character (see Ref 9), whereas temperature values at points in the solid that are not close to the melt pool are influenced by both upstream and boundary conditions. These general characteristics of the system provide a mathematical basis for *uncoupling*, for the purpose of calculating thermal cycles, two regimes of the unsteady welding process. One regime is of heat conduction and fluid flow in the region of the workpiece associated with the keyhole, melt pool, and surrounding heated solid. The other regime is of heat conduction in parts of the workpiece that are in the solid phase where the influence of upstream conditions in the system are comparable to that of downstream conditions. This regime would include a large fraction of the heat-affected zone.

The approach of using a steady-state configuration of the solid/liquid interface, discussed in Section 6, is an approximation in that the heat of fusion will introduce local thermal gradients in the neighborhood of this surface. As a result, isothermal surfaces that are near the liquid/solid interface are time dependent even if the system has reached a steady state globally. An examination of this property is given below and is based on an analysis of the time dependence of local shape changes of the isotherm labeled "c." For this model, this isotherm is within a

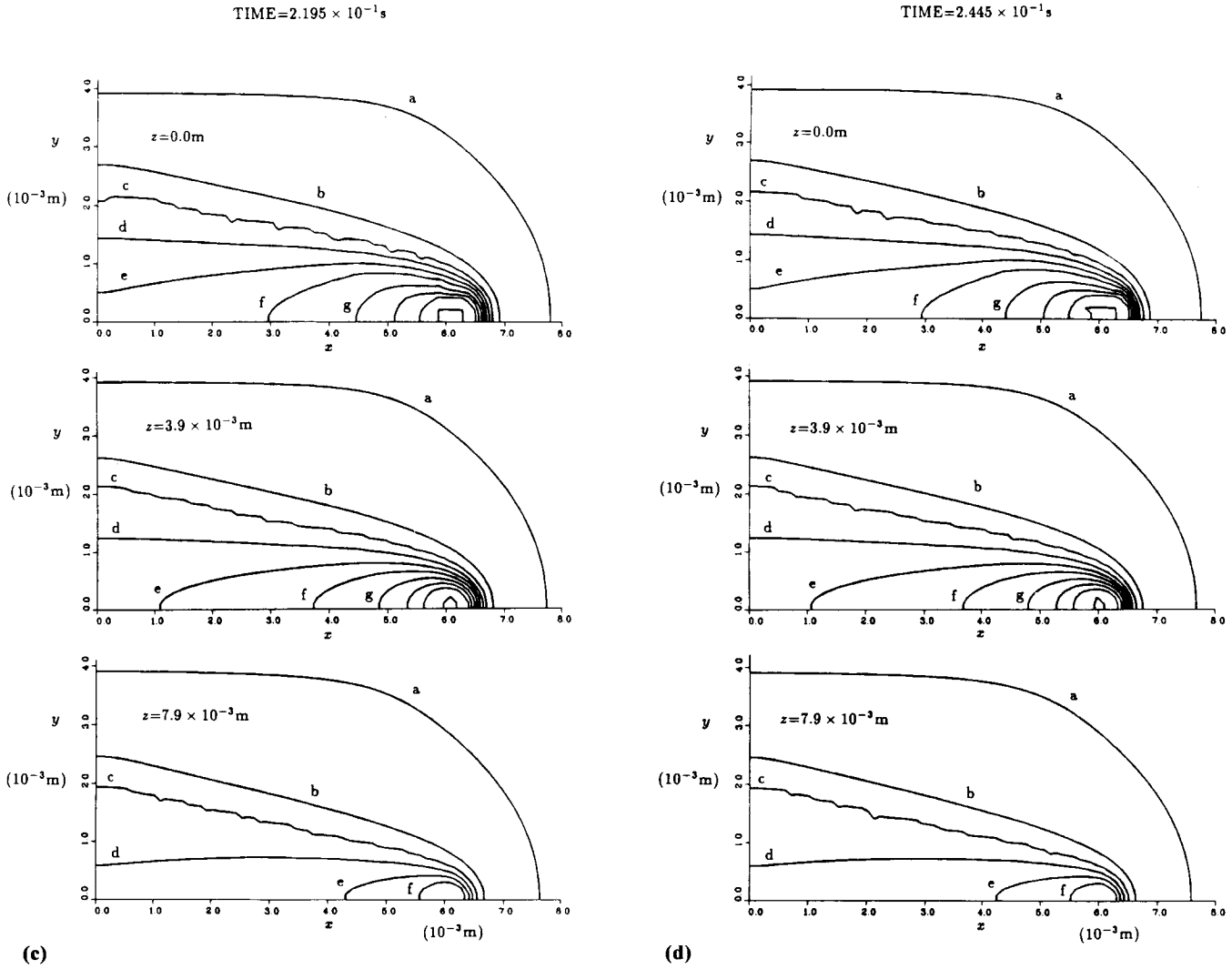

Fig. 8 Unsteady evolution of model system to steady state for both temperature and fluid velocity field. The temperatures of isotherms are assigned as in Fig. 6.

(continued)

temperature range for which there is exothermic energy release (represented in the current model by large changes in the value of C_p for temperatures near $T = 1000$ K). Therefore, in the present simulations, the shape of the isotherm labeled "c" (in contrast to other isotherms that are shown) is time dependent even when the system has reached a steady state.

7. Sample Calculations of Thermal Cycles for Elements of Prototype Iron-Steel System

In this section, a sample calculation is described of steady-state thermal cycles, $T(x,y,z,t)$, for elements of the model system. These thermal cycles are shown in Fig. 9(a) through (f). One purpose of these calculations in the present study is to examine the numerical aspects of the model for its extension to the quantitative analysis and prediction of welding structures that could occur in complex welding processes. Another purpose is to examine the general influence of energy changes associated with solid-state transformations and their significance in calculating thermal cycles.

In the present study, to isolate the general features of local energy changes due to reactions, the authors have not incorporated into the model system any general transformation effects. In the present simulations, local energy changes due to melting, solidification, or any specific exothermic (or endothermic) solid-state reaction that would occur in a specific alloy has not been considered. In the present analysis, only a single exothermic reaction that occurs at temperatures in the neighborhood of 1000 K and is independent of whether or not the workpiece element is cooling or heating has been considered. The spatial and temporal character of structures due to this prototype reaction should be reasonably representative of structures associated with solid-state reactions or phase transformations.

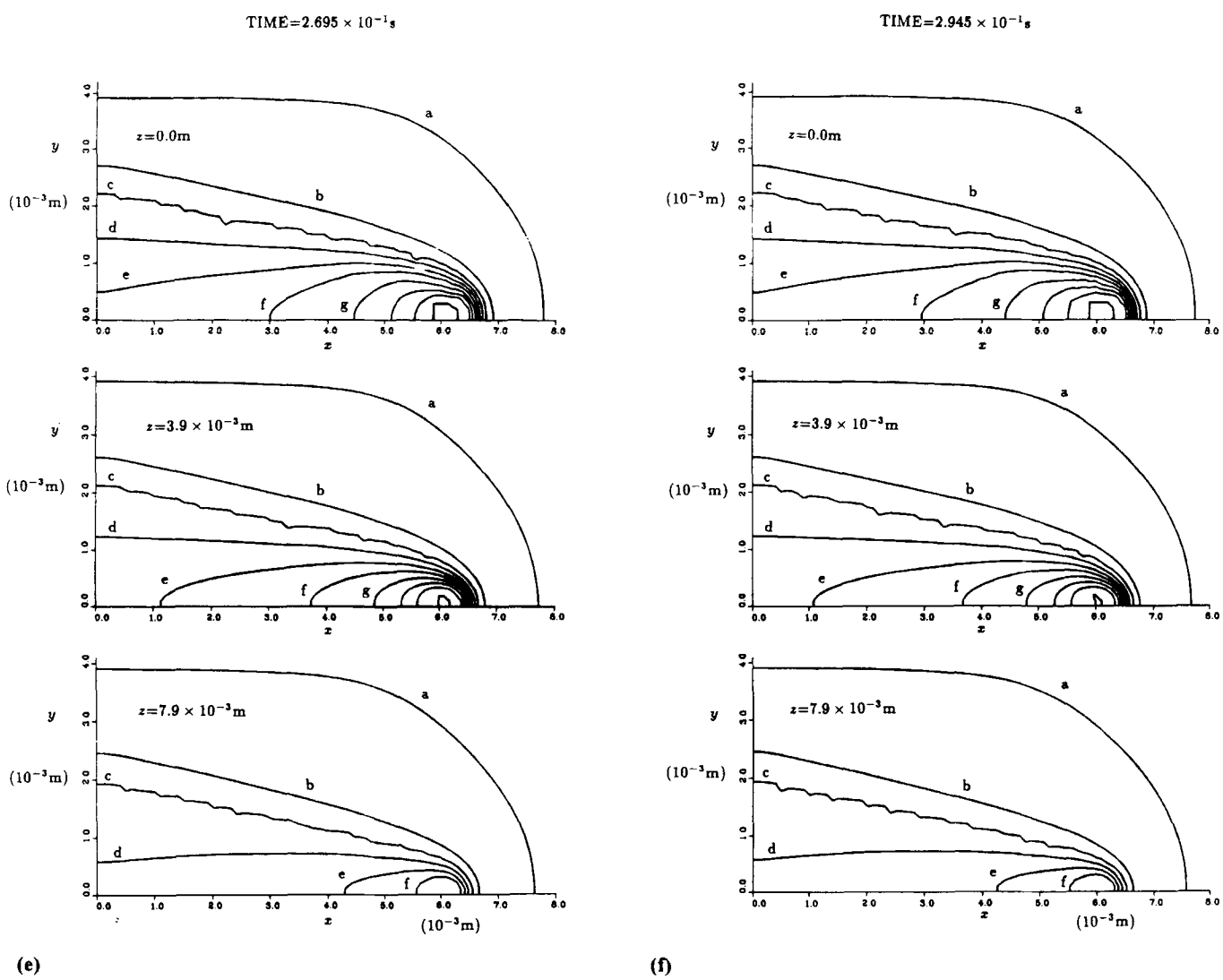

Fig. 8 Unsteady evolution of model system to steady state for both temperature and fluid velocity field. The temperatures of isotherms are assigned as in Fig. 6.

The thermal cycles shown in Fig. 9 are calculated from the steady state of the system whose temperature field is shown in Fig. 8(f) according to the relation

$$T(x,y,z,t) = T\left(x,y,z,\frac{x}{V_B}\right) \qquad [37]$$

Several aspects of this calculation merit comment. In the present calculation, the accuracy of the calculated T and U_j fields decreases for values progressively closer to the keyhole as does the accuracy of the T field in the neighborhood of the isotherms labeled "c." For the purpose of this initial study, a series of simulations were performed that combine three regions of the workpiece, each containing different structures whose characteristic time and length scales may be dissimilar. In addition, only the thermal cycles $T(x,y,z,t)$ were calculated for t less than 0.14 s. In a more quantitative analysis, the thermal cycles can be extended indefinitely in time by adopting the time-dependent boundary values of the temperature field (Eq 17b and 18a) as in-flow boundary conditions on model systems that represent adjoining parts of the workpiece. For elements of the workpiece that are relatively far from the beam source and whose temperatures are in the range of values for which $T(x,y,z,t)$ corresponds to cooling, sufficient grid resolution is required for an accurate calculation of time-dependent structures due to phase transformations. As discussed above, the inherent weak coupling between the regions of the workpiece that are and are not near the melt pool permit an efficient partitioning of the calculation into separate calculations. Similarly, there is a weak coupling between regions of the workpiece where exothermic or endothermic changes in energy do and do not occur, thus permitting further partitioning of the system and of the associated calculations. Of course, in principle, in-

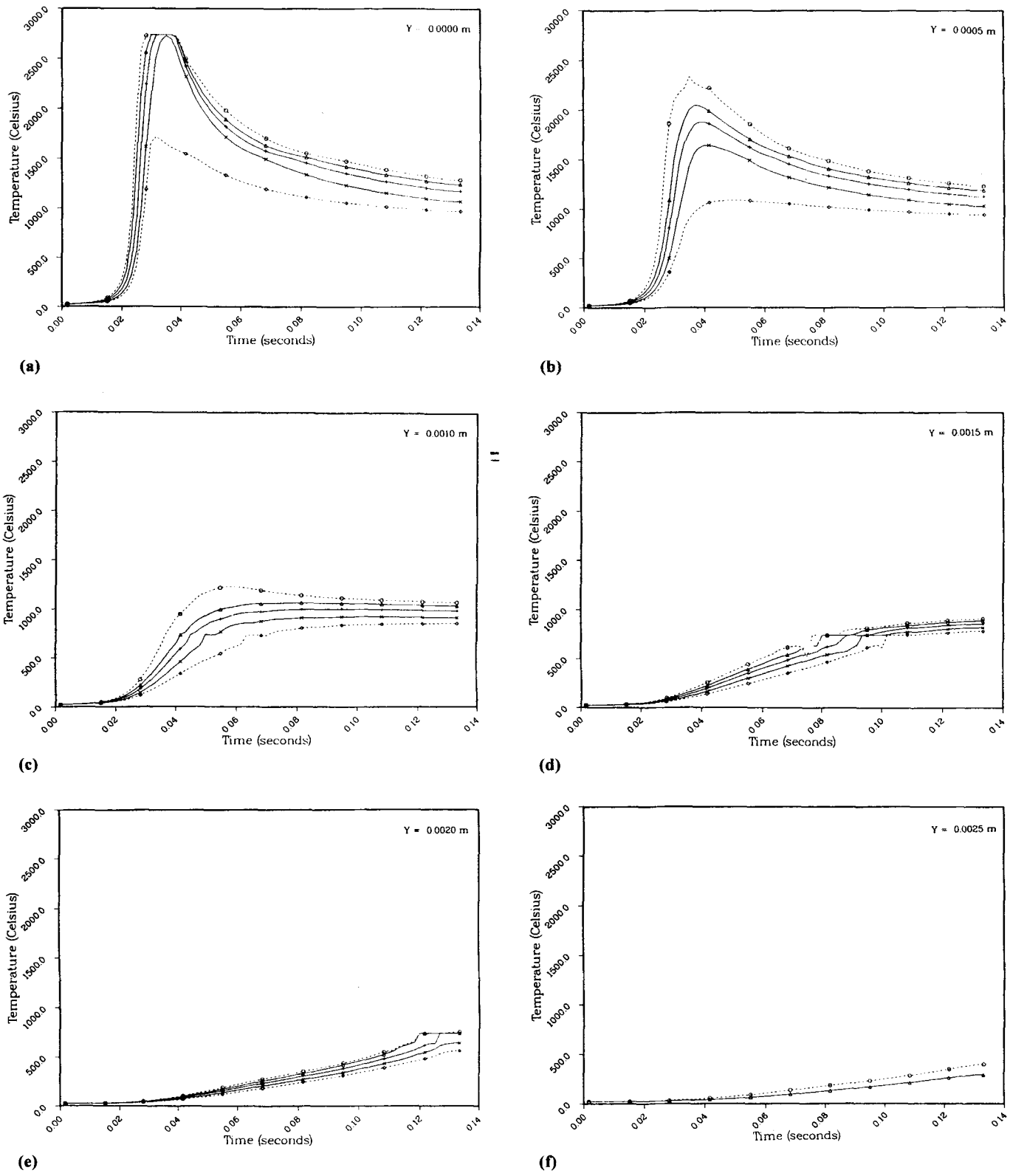

Fig. 9 Steady-state thermal cycles for different elements of model workpiece. These thermal cycles were calculated using the steady state shown in Fig. 8(f) according to the relation $T(x,y,z,t) = T(x,y,z,V_B x)$. The thermal cycles shown in each of these figures (each corresponding to a specified xz plane) correspond to different depths within the workpiece and are labeled as follows. The circles denote $z = 0.0$ m (top surface of workpiece); the triangles denote $z = 0.002$ m; the plus signs denote $z = 0.004$ m; the × denotes $z = 0.006$ m; and the squares denote $z = 0.008$ m (bottom surface of the workpiece).

creased accuracy can be obtained for the combined calculation via embedded meshes at an increase in computational cost. Finally, Eq 37 is not valid for steady-state structures that are time dependent. This is discussed below.

It is important to note the significance of the unsteady-state calculations for the calculation of steady-state structures and for the calculation of unsteady structures in general. For the steady-state calculation shown by Fig. 8(f) and 9, it is not necessary to calculate the precursor unsteady system states with a level of accuracy comparable to that of those system states in the time neighborhood of the steady state. In the context of a steady-state calculation, the unsteady precursor states serve only as initial estimates. The steady-state temperature and fluid velocity fields depend only on the steady-state shape of the keyhole vapor/liquid boundary for a given welding speed. It follows then that, for a steady-state calculation, any model for the unsteady evolution of the keyhole boundary can be adopted, even one that is unrealistic, as long as its final configuration is physically accurate. If the unsteady evolution of the melt pool is important, then a more quantitatively accurate representation of the temporal or unsteady character of the keyhole liquid/vapor interface must be included in the model system. It is observed experimentally, for example, that the unsteady evolution of the keyhole boundary occurs on a timescale that is much shorter than that shown in Fig. 6. Thus, the beam parameter values used here, i.e., the values of β_b and Q_0, for modeling the unsteady evolution of the keyhole may serve more as a generator of successively better estimates of the steady-state keyhole boundary rather than a model for keyhole evolution.

An issue whose consideration can be important for calculating quantitatively accurate thermal cycles and for using numerical model simulation to predict weldment structure concerns the highly localized variations of the function $T(x,y,z,t)$ shown in Fig. 9. These highly localized variations of $T(x,y,z,t)$, which are particularly noticeable in Fig. 9(c), (d), and (e), are due to energy release at temperatures within a relatively narrow range. This energy release is modeled via the addition of a temperature-dependent term to the heat capacity function, C_p. This term is weakly dependent on temperature, i.e., it varies slightly with temperature, except for approximately a 100-degree interval centered at 1000 K (727 °C), where it rises and falls sharply with changing temperature. In the present analysis, the general behavior of structures due to this prototype exothermic reaction are considered in that the time and length scales for the associated energy deposition are typical of solid phase reactions or energy changes at the fusion boundary.

An analysis of the unsteady evolution and local time dependence of an isothermal surface, e.g., the isotherm labeled "c," within the temperature range for which there is an exothermic reaction provides a case study examination of the influence of local energy release. Referring to Fig. 6(a) through 7, and 8(a) through (f), note that all isotherms are smooth, except those labeled "c," where temperature is within the range of values for which there is an exothermic reaction. There are two important aspects of this highly localized structure that must be considered to increase the accuracy of the numerical simulation. These two aspects are the mathematical character of this structure, i.e., the characteristic space and time scales of this structure and how these scales determine the computational requirements of its accurate calculation, and the physical character of this structure and the nature of its coupling to the overall welding process.

The characteristic length and time scales of this structure are such that a higher level of both temporal and spatial resolution is required relative to that for calculation of the surrounding temperature field. However, by comparing the calculated temperature for different times that are close to steady state, e.g., Fig. 8(c) through (d), it is evident that the time-dependent structures occurring in the neighborhood of isotherm c are relatively local and do not influence the shape of other isotherms. In addition, for a given isotherm, these structures may be characterized by relatively small deviations from a time-averaged steady-state temperature. Therefore, thermal cycles calculated from a given steady-state configuration of the system according to Eq 37 should represent a reasonably good approximation. Local spatial resolution can be increased by local grid refinement via the embedded mesh method discussed above.

An extension of the present model system for detailed calculations of thermal cycles for individual elements of a workpiece can include information about transformations if that information is available. The practical implementation and feasibility of this approach is an open issue for further research.

8. Analysis of Fluid Velocity Field due to Keyhole Stirring

Fluid velocity fields along various two-dimensional slices of the model three-dimensional workpiece are shown in Fig. 10. The velocity fields shown in Fig. 10 correspond to the system state whose temperature field is shown in Fig. 7 and which does not include surface tension. The velocity fields shown in Fig. 10 are in a coordinate frame of reference whose origin is stationary with respect to the beam. The physical effect to be noted is the relative increase in the velocity of the liquid near the keyhole boundary. For this calculation, the average speed up of the fluid relative to the workpiece is approximately half the welding speed, or equivalently, an increase in speed that is on the order of twice the welding speed, V_B, in the reference frame of the beam. The result is predicted by laminar flow theory[12] and is consistent with the value of viscosity used in this calculation, i.e., a low Reynolds number. In a preliminary calculation using this model, beam parameters of $R_b = 2 \times 10^{-3}$ m and $V_B = 10^{-2}$ ms^{-1} are used. For these parameter values, the resulting weld pool size is sufficiently large such that the keyhole boundary is separated from the liquid/solid boundary. In this case, the liquid/solid boundary has less of an impeding influence on the flow. For this calculation, the maximum speed is 0.0206 m/s relative to the beam and is very close to twice the welding speed.

The presence of the keyhole represents a geometric constraint on the flow of the fluid rather than a driving force. This constraint causes increases in the velocity of the fluid by factors close to two and is independent of the nature of the forces driving flow at points in the liquid that are not in the neighborhood of the keyhole boundary, e.g., buoyancy or surface tension. This implies that the presence of the keyhole is always a domi-

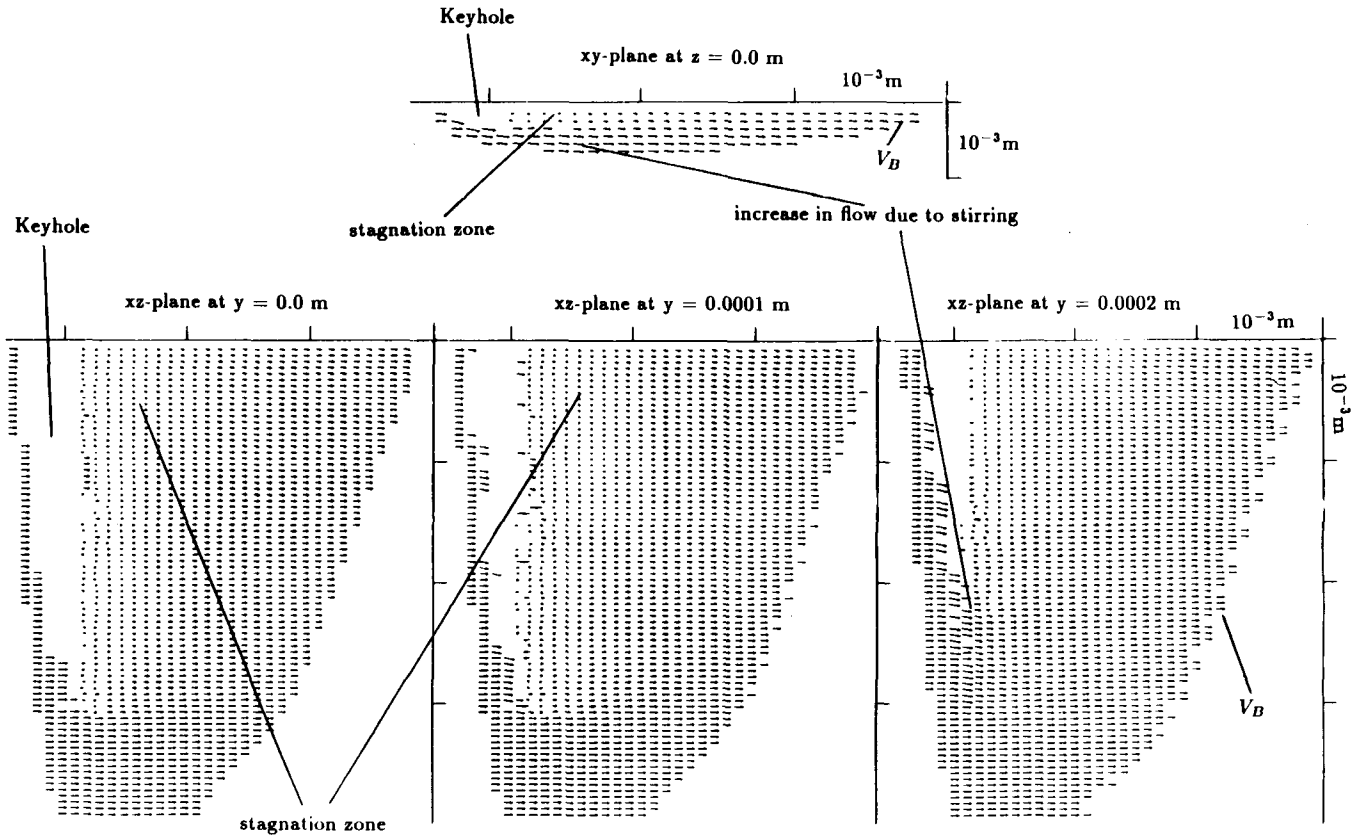

Fig. 10 Fluid velocity field showing the effect of keyhole stirring. The velocity field shown is for the system state shown in Fig. 7.

nant influence on fluid convection and that its shape plays an important role.

9. Discussion and Conclusion

A numerical model and associated general approach for simulating the combined system of keyhole, melt pool, and heated solid in both steady and unsteady deep penetration welding processes have been presented. The calculations presented in this study are for the purpose of demonstrating the generality of this approach and of showing the dominant characteristics of deep penetration welding processes that are significant for accurate modeling. Although the beam energy source used in this initial study is that of a continuous beam, the results presented here should be representative of welding processes associated with laser and electron beams with different temporal behavior. In addition, an overview of the important features of the numerical methods used in the model has been presented, with discussion of how these features contribute to its flexibility for simulating different types of welding processes. Extensions of the model according to these features have been suggested.

An extension of the model system for a more detailed analysis of deep penetration welding of metals should include a more detailed representation of the liquid metal properties. Experimental and theoretical studies[13,14] indicate that, over the range of temperatures between T_M and T_G, the viscosity and density of liquid metals varies significantly. For example, the density of liquid iron varies by 15% for T in (T_M, T_G). Therefore, assuming a constant viscosity and density may not be an accurate approximation for characterizing fluid flow around the keyhole. A better understanding of the include of the keyhole requires extending the current model to include effects associated with compressibility and changes in viscosity as a function of temperature.

The deposition of energy on the time-dependent boundary according to a power distribution law is phenomenological in that it is a representation which implicitly assumes the nature of the coupling between energy deposition on the surface of the keyhole and processes occurring inside the keyhole. A more quantitative study should take an accurate account of this coupling. The approach used in the model, i.e., time-dependent boundaries, however, does suggest a tractable approach toward consideration of this coupling. Experimental observation shows that the keyhole surface is typically unsteady and that a detailed consideration of processes inside the keyhole may require a substantial computation cost in addition to the typically high level of computation associated with the numerical modeling of processes involving three-dimensional fluid flow and heat conduction. Experimental observations also suggest, however, that a quantitative description of the temporal behavior of the keyhole can be determined and that this information can be included in a model via time-dependent boundary conditions

and thus represented on a time scale characteristic of unsteady flow structures that can occur in a weldment.

The important physical and numerical features of the model system discussed in this paper are reviewed, and the issues related to its extension to more detailed and quantitative analysis of welding structures are discussed. These features include the following. The stirring action of the keyhole represents the overwhelmingly dominant influence on fluid flow in deep penetration welding. The local character of the beam source in deep penetration welding is such that other influences on fluid flow, e.g., surface tension, are small relative to stirring because of the relatively rapid onset of solidification.

The steady state of the weld pool is weighted primarily by the upstream conditions of the system and therefore achieves a steady state rapidly relative to the time for achieving a steady state of the total welding process. The deep penetration welding process consists of multiple regimes, both in the fluid and solid, whose characteristic time scale are dissimilar. The formalism of the SIMPLE algorithm (although moderately optimal for modeling structures in particular regimes) is highly adaptable to modeling the combined system.

The different regimes comprising the total welding process tend to be weakly coupled, thus permitting a partitioning of the system for the purpose of calculating structure.

The welding process can consist of time-dependent structures, even in the steady state, and therefore (in cases where such information is available and can be put into the model, e.g., Eq 7) a detailed calculation of thermal cycles must track individual elements in time. The welding process consists of many spatially fine structures that are embedded into coarser structures. The SIMPLE algorithm is easily combined with the method of embedded meshes for local grid refinement. Given an accurate thermal cycle $T(x,y,z,t)$ for elements of a workpiece, weldment characteristics can be predicted.

Acknowledgment

The authors would like to thank the ONR for sponsorship of earlier stages of this research and DARPA for its sponsorship of an effort for extending this research. In addition, the authors would like to thank R. Dixon, G. Lewis, and J. Milewski of the Metallurgy Group at the Los Alamos National Laboratory for their discussions about deep penetration welding and for their continued collaboration in this modeling effort. Furthermore, the authors would like to thank R. Guirguis of the Naval Surface Warfare Center at White Oak, Maryland, for his discussions about computational fluid dynamics. One of the authors (A. Monis) would like to thank the SEAP program of the Naval Research Laboratory for their support in this effort over the past 2 years. And finally, another of the authors (S.G.L.) would like to thank L. Phillips for his discussions about transport phenomena.

References

1. S. Kou, *Welding Metallurgy*, John Wiley & Sons, 1987, p 9
2. Y.H. Wang and S. Kou, Modelling and Control of Casting and Welding Processing, *Proc. 3rd Conf. Modelling of Casting and Welding Processes*, S. Kou and R. Mehrabian, Ed., The Metallurgical Society, 1986, p 197
3. J.F. Lancaster, *The Physics of Welding*, Pergamon Press, 1986, p 146-221
4. R. Dixon, G. Lewis, and J. Milewski, Los Alamos National Laboratory, private communication, 1992
5. E.A. Metzbower, Laser Beam Welding: Thermal Profiles and HAZ Hardness, *Weld. J.*, Vol 69 (No. 7), 1990, p 272
6. E.A. Metzbower, Experimental Laser Weld Thermal Cycles, *J. Laser Appl.*, Vol 1 (No. 3), 1987, p 9
7. M.C. Tsai and S. Kou, Power Beam Processing (Electron, Laser, Plasma-Arc), *Proc. Int. Power Beam Conf.*, E.A. Metzbower and D. Hauser, Ed., ASM International, 1988, p 131
8. J.M. Glass, H.P. Groger, R.J. Churchill, and E.M. Norin, Laser Cutting of Amorphous Alloy Ribbon, *J. Mater. Eng.*, Vol 12 (No. 1), 1990, p 59
9. S.V. Patankar, *Numerical Heat Transfer and Fluid Flow*, Hemisphere Publishing, 1980, p 126-130
10. D.F. Watt, L. Coon, M. Bibby, J. Goldak, and C. Henwood, An Algorithm for Modelling Microstructural Development in Weld Heat-Affected Zones, *Acta Metall.*, Vol 36 (No. 11), 1988, p 3029
11. C.M. Albone and G. Joyce, *Proceedings of the Eleventh International Conference on Numerical Methods in Fluid Dynamics*, Springer-Verlag, 1989, p 106
12. R.B. Bird, W.E. Stewart, and E.N. Lightfoot, *Transport Phenomena*, John Wiley & Sons, 1960, p 136-137
13. Z. Morita and T. Iida, Viscosity of Molten Iron and Steel, *Proc. 1st Sino-Japanese Symp. Iron and Steel*, Chinese Society of Metals, 1981, p 103-127
14. T. Iida and R.I.L. Guthrie, *The Physical Properties of Liquid Metals*, Oxford University Press, 1988, p 70